

Chapter 2

The Mariner 10 Era of Mercury Science

2.1 Introduction

In this chapter I want to summarise what we found out about Mercury as a result of Mariner 10 and the ground-based observations (principally radar and spectroscopy) carried out until the first few years of the current century. It is thus a snapshot of Mercury knowledge in the immediate pre-MESSENGER era, when we had seen almost half of Mercury in close-up and had amassed a certain amount of geophysical data. I will try to avoid presenting as ‘the truth’ any Mariner 10 era interpretations that we now know to be incorrect.

Let’s begin by looking at the Mariner 10 mission.

2.2 Three Flybys for the Price of One

2.2.1 *The Trajectory*

Mariner 10 (Fig. 2.1) was the first space probe to visit Mercury, and the seventh successful launch in NASA’s Mariner series. The Mariner craft shared a common heritage, being based on a hexagonal or octagonal ‘bus’ housing the electronics and with components such as communications antennae, cameras, solar panels and thrusters attached. Mariners 1 (failed), 2 and 5 were Venus flyby missions, Mariners 3 (failed), 4, 5 and 6 were Mars flybys, and Mariners 8 (failed) and 9 were Mars orbiters. Mariners 11 and 12 had been planned as Mariner Jupiter-Saturn probes but were superseded by extensively redesigned probes that became Voyager 1 and Voyager 2.

At 502 kg, Mariner 10 was more than twice the mass of the first Mariners, but considerably less massive than the 998 kg Mariners 8 and 9. It was launched on 3 November 1973, spent 25 min in a parking orbit, and was then sent on its way toward Mercury powered by a hydrazine rocket capable of 222 N of thrust.



Fig. 2.1 Mariner 10 as it would have looked in flight. Each solar panel was 2.69 m long, and housed three pairs of orthogonal nitrogen gas reaction thrusters to control and stabilize the spacecraft's attitude. The arm extending to the left is the magnetometer boom, which was 5.8 m long. The flat white dish is the sunshade, through which the main engine's nozzle (invisible) projected. The steerable high-gain antenna for communications sticks out beyond the sunshade. The shorter arm houses the omnidirectional low gain antenna (NASA)

There was a scare after 10 days. Following a trajectory correction manoeuvre, the craft's star-tracker locked onto what is now presumed to have been a speck of paint that had flaked off the spacecraft, mistaking it for the guide star, Canopus. Fortunately this was rectified, and Mariner 10 continued on the correct path. In January 1974 the Mariner 10 team took advantage of an opportunity to make 15 days of continuous distant ultraviolet observations of the long-period comet Kohoutek, which had been discovered only 9 months before launch and was by now just past perihelion. On 5 February Mariner 10 made the closest yet flyby of Venus, at a range of less than 6,000 km. Its ultraviolet imaging of Venus revealed structure in the cloud deck that had hitherto seemed featureless, and its magnetometer showed that Venus has no significant magnetic field of its own.

Although the science that Mariner 10 achieved at Venus was important, the Venus flyby had an entirely different purpose. This was to use Venus's gravity to bend Mariner 10's trajectory so that it was now following a heliocentric orbit with a perihelion that would coincide with Mercury's position at the time of its coming encounter (Fig. 2.2). This had been timed to occur at Mercury's aphelion so that the spacecraft would not have to go any closer to the Sun than necessary, thereby reducing the risk of overheating.

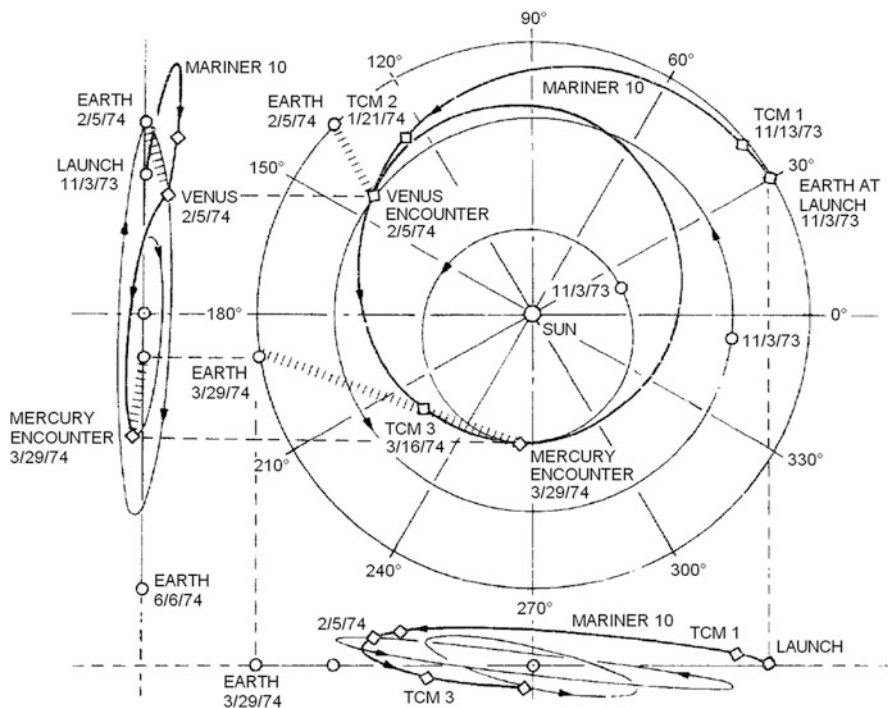


Fig. 2.2 A diagram copied from a 1976 NASA technical manual, illustrating the trajectory of Mariner 10. The main graphic shows a plan view of the orbits of Earth, Venus and Mercury plus the position of each planet at launch (with dates expressed in the American month/day/year format: 11/3/73 for 3 November 1973). Also shown are positions of three planned trajectory correction manoeuvres (TCM), the positions of Earth and Venus during Mariner 10's Venus flyby, and the positions of Earth and Mercury during Mariner 10's first Mercury flyby. Graphics at side and bottom show projections of the trajectory viewed side-on to Earth's orbital plane (the ecliptic), reminding us that Mariner 10 had to escape from this plane to accomplish its flybys of Mercury (NASA)

Mariner 10's swing past Venus was the first ever execution of a 'gravitational slingshot manoeuvre', also known as a 'gravity assist trajectory'. This is a technique now widely used in missions to both the inner and outer parts of the Solar System. By accelerating a spacecraft into a more suitable trajectory, it enables a spacecraft to fly with less fuel so that it can carry a greater mass of scientific instruments.

The precise gravity assist trajectory chosen for Mariner 10 did more than merely setting up a flyby of Mercury at the right time. Giuseppe (known as 'Bepi') Colombo, Professor of Applied Mechanics at the University of Padua, Italy (Fig. 2.3), had made an insightful suggestion at a conference on the Earth-Venus-Mercury mission held in Pasadena in 1970. As a result of this, the gravity assist from its first Mercury encounter was used to place Mariner 10 in an orbit about the Sun with a period exactly twice that of Mercury. With no further expenditure of rocket fuel (which was by now pretty much exhausted anyway), Mariner 10 would orbit the Sun and return to the same point 176 days later to find Mercury, having gone twice round the in the meantime, there again.



Fig. 2.3 Two people whose insights made missions to Mercury feasible. *Left:* Giuseppe Colombo, who proposed the 2:1 probe:Mercury resonant solar orbit achieved by Mariner 10. *Right:* Chen-wan Yen, who found a low-cost trajectory to get a probe into orbit about Mercury, as used by MESSENGER and BepiColombo (Left courtesy of ESA, right courtesy of Chen-wan Yen)

In fact Mariner 10 made three successful flybys of Mercury. The first, 29 March 1974, passed at closest only 704 km above Mercury's surface. The second, 21 September 1974, was at a more distant 48,069 km but allowed the south polar region to be imaged. The third, 16 March 1975 at a closest altitude of 327 km, was achieved only after recovery from another temporary loss of star tracking (probably another floating speck of paint), and tilting of the solar panels to control the roll of the spacecraft so as to conserve precious attitude-control gas. The gas became totally depleted 9 days after the third fly-by. Mariner 10 then began slowly to tumble uncontrollably. There being no means to correct this, commands were sent to the spacecraft to turn off its transmitter. This ended Mariner 10's contact with Earth forever, though presumably it still passes close to Mercury at every perihelion of its lonely orbit.

2.2.2 Limitations

Despite achieving three flybys for the price of one, Mariner 10 data acquisition was not without its problems. The onboard tape recorder failed soon after the first flyby, which meant that data from subsequent flybys had to be transmitted to Earth in real time. This required the use of multiple tracking station antennae in parallel to overcome the noise problems inherent in such weak signals transmitted at the necessary data rate. During the third flyby, Mercury was below the horizon, and so unobservable, from the Goldstone tracking station in California. Only the Canberra Deep Space Network station could see Mercury, but this developed a problem with a cooling system that had been intended to reduce receiver noise. To make the best of

the situation, Mariner 10 had to be instructed to transmit only narrow strips of images, rather than full frames of the high resolution targeted images that had been selected on the basis of the most interesting areas seen in the first flyby.

Further limitations to Mariner 10's study of Mercury's surface had nothing to do with hiccups in the technology. These relate to Mercury's 3:2 spin orbit coupling. Because Mercury completed exactly two orbits of the Sun between flybys, it had meanwhile rotated exactly three times and so experienced exactly 1 solar day (Fig. 1.7). Therefore the same hemisphere was in darkness during each flyby, and so could not be seen at all. In total about 40–45 % of the globe was imaged well enough to attempt mapping, using a total of about 2,800 images.

For mapping, and even simply to understand the surface features, the position of the Sun in the sky is important. At high 'Sun angle', when there is a large angle between the Sun and the local vertical, the Sun is fairly close to the local horizon, so the sunlight strikes the ground obliquely. This casts shadows that can reveal subtle topographic features with great clarity. It is the preferred illumination condition for many purposes, though of course you can see nothing inside the shadows and so most geologists would prefer to complement this with a second high Sun angle pass with the sunlight coming from the opposite side. On the other hand, when the Sun is high in the sky (described as conditions of low Sun angle, because there is only a small angle between the Sun and the local vertical) the whole of the ground is bathed in sunlight, revealing differences in surface reflectivity that are suppressed under high Sun angle conditions. However, in the absence of shadows or subtleties of shading brought about by such illumination, the topography can be very indistinct. Figure 2.4 shows an example of the different information revealed according to Sun angle.

2.3 Mariner 10's Instruments

Mariner 10 did more than just send back images from Mercury. It carried a total instrument payload of 79.4 kg, designed to contribute to seven scientific experiments. These are listed in Table 2.1 and described below.

2.3.1 *Television Science*

The now rather quaint-sounding 'Television science' experiment was so-named because it used what were effectively TV cameras (vidicons) to obtain its images. The imaging system was mounted on a steerable scan platform to allow accurate pointing and construction of image mosaics without having to re-orient the whole spacecraft. Long focal length fore-optics (the telescopes) were fitted because for the first and third flybys the closest approach to the planet would be on the night-side. High magnification was therefore needed to achieve high-resolution (detailed) images while the sunward part of the globe was in view, before and after the closest stages of the inward and outward legs of the flyby (Fig. 2.5).

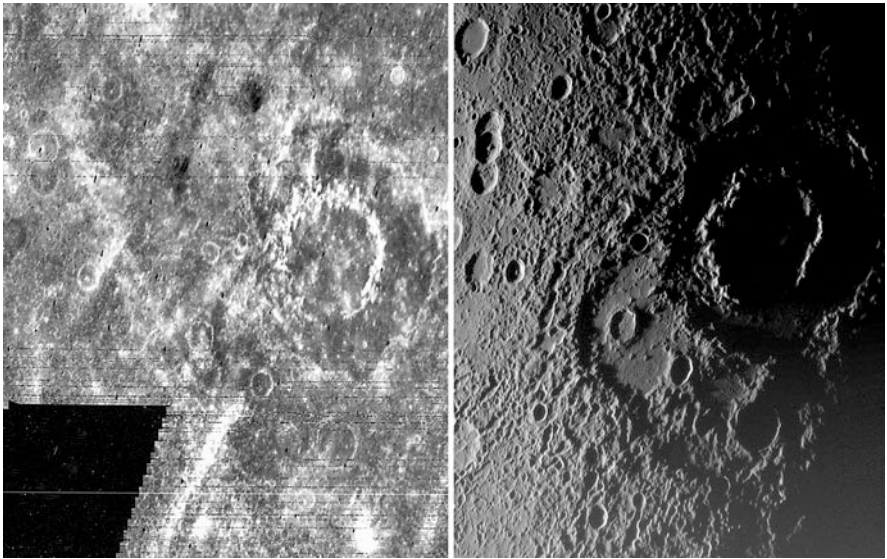


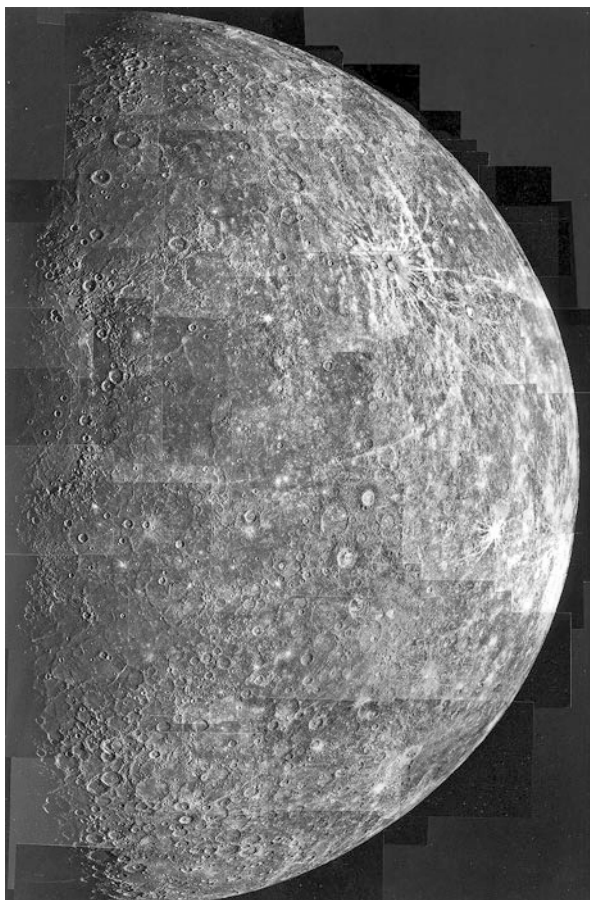
Fig. 2.4 Mariner-10 (*left*) and MESSENGER (*right*) views of the same area of Mercury. The 200 km diameter peak-ring crater Vivaldi is prominent on the right of each image. Mariner-10 saw this area with the Sun nearly overhead (low Sun angle) so albedo features are prominent, but topography is suppressed. The bright streaks are mostly ejecta rays: the one in the lower left (adjacent to the missing data) is from Vivaldi itself, but others can be traced to craters as distant as 2,000 km. The MESSENGER image, acquired during its first flyby in 2008, shows the same area shortly before sunset (high Sun angle) so topography is clearly seen. This comparison does Mariner 10 somewhat of an injustice, because high Sun angle Mariner 10 images (not available at this longitude) are almost as attractive as MESSENGER high Sun angle images (NASA)

Table 2.1 Mariner 10’s seven scientific experiments and the relevant instruments

Experiment	Instrument
Television science	Vidicon cameras fitted to twin 1.5 m focal length telescopes
Infrared radiometry	Infrared radiometer
Ultraviolet spectroscopy	Airglow spectrometer and occultation spectrometer
Celestial mechanics and radio science	X-and S-band radio transmitters
Magnetic field	Two triaxial fluxgate magnetometers
Plasma science	Scanning electrostatic analyser and electron spectrometer
Charged particles	Charged particle telescopes

The spatial resolution in the images used for Fig. 2.4 was 2–4 km, but resolution as high as about 100 m was achieved for small areas at about 30 min either side of closest approach. The second flyby passed over the south polar region, acquiring images that enabled the inbound and outbound image sequences from the first flyby to be fitted together with cartographic accuracy.

Fig. 2.5 Photomosaic of the hemisphere of Mercury seen by Mariner 10 outbound from its first flyby. I have adjusted the contrast to reveal detail near the terminator without saturating the more brightly-lit region near the limb. The sunlit half of the Caloris basin straddles the equator on the terminator (NASA)



A full image frame consisted of 700 scan lines of 832 pixels each, and could be recorded through any of five filters, which were mounted on a filter wheel deployed between the telescope and the vidicon. Filters were 'clear', ultraviolet (UV, central wavelength 355 nm), blue (central wavelength 475 nm), 'minus-ultraviolet' (MUV, central wavelength 511 nm) and orange (central wavelength 575 nm). There was also a polarizing ultraviolet filter used only at Venus. Colour information obtained at Mercury was poor, and generally has to be inferred from the orange albedo and the UV/orange ratio.

2.3.2 *Infrared Radiometry*

The main purpose of this experiment was to measure infrared radiation emitted from the surface of Mercury, and thus to determine surface temperature. It was

based on two 2.5 cm aperture telescope radiometers, one sensitive to 8.5–14 μm and the other to 34–55 μm radiation. Unlike the television science experiment, this was not steerable but was mounted on the spacecraft so as to allow nearly perpendicular viewing onto the night side of Mercury plus the inbound and outbound terminators. This was not an imaging experiment, but merely recorded radiation as the radiometers' 0.5–1° fields of view tracked across the planet.

During the first flyby, the two radiometers measured how temperature varied along a near-equatorial line beginning shortly before local sunset and extending through midnight to end well after dawn (approximately 1700 to 0900 'local time' on the surface). The experiment determined that Mercury's surface physical properties controlling its rate of day-night heating-cooling were essentially indistinguishable from those of the Moon.

2.3.3 Ultraviolet Spectroscopy

The airglow spectrometer searched for UV emission at discrete energies associated with specific gas species. In the event, it was able to measure H, He and O (atomic hydrogen, helium and oxygen), and placed upper limits on the possible abundances of Ne, Ar and C (neon, argon and carbon).

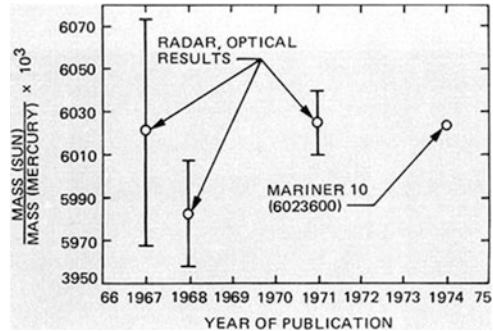
The occultation spectrometer was designed to look at the Sun in the 30–95 nm region (a part of the spectrum where any gases would scatter/absorb sunlight most strongly) as it was occulted by Mercury's limb, to search for absorption by any atmospheric gases. In the event, no measurable absorption was found, placing an upper limit on Mercury's atmospheric density.

2.3.4 Celestial Mechanics and Radio Science

This experiment was designed to extract scientific information from the dual-frequency X-band and S-band radio transmissions from Mariner 10 that were used to send data to Earth. The celestial mechanics part of the experiment was based on determining slight Doppler shifts in the received wavelengths while the spacecraft was accelerated by the competing gravitational tugs of Mercury and the Sun. This measured the mass of the planet to far greater precision than ever before (Fig. 2.6), and gave some hints about its internal mass distribution.

The radio science part of the experiment considered the signals as Mariner 10 passed behind Mercury as seen from the Earth. This provided a check on the planet's size, and together with the celestial mechanics data confirmed Mercury's density at the currently accepted value. In addition, the lack of attenuation of the signal when the line of sight approached the planet put upper limits on the electron density in any ionosphere and on the surface atmospheric pressure.

Fig. 2.6 Published values of the ratio between the Sun's mass and Mercury's mass as measured by radar and optical methods, with error bars, and the much more precise determination by the Mariner 10 celestial mechanics experiment, published in 1974 (NASA)



2.3.5 Magnetic Field

Before Mariner 10, it was widely assumed that Mercury was too small for any zone in its core to be hot enough to be molten, because the higher surface-to-volume ratio of a smaller planet allows it to lose more of its internal heat than a larger planet. It was further reasoned that Mercury's rotation is too slow to stir any molten core into the kind of motion necessary to generate an Earth-like magnetic field. With these considerations in mind, Mariner 10's magnetic field experiment was expected to observe the interaction between Mercury and the solar magnetic field, and the extent to which the charged particles in the solar wind were able to induce a secondary magnetic field inside the planet.

Mariner 10 carried two magnetometers, one halfway along and one at the end of its magnetometer boom to allow any spacecraft-induced secondary magnetic fields to be identified and eliminated. These were triaxial fluxgate magnetometers, each capable of measuring the strength and direction of the local magnetic field in three orthogonal directions. By summing the three measurements, this gave the strength and direction of the field in three-dimensional space.

Strong hints of a powerful, internally-generated magnetic field during the first flyby of Mercury, which were confirmed in the third flyby, provided a major surprise, especially after none had been found at Venus. Mariner 10 did not pass inside Mercury's magnetosphere during its more distant, and dayside polar, second flyby.

2.3.6 Plasma Science

This experiment comprised an ion and electron analyser scanning in the sunward direction (the electrostatic analyser) and an electron spectrometer looking in the antisun direction. Unfortunately the electrostatic analyser failed, so no data about the ion population were acquired. However, useful data came from the electron spectrometer, which measured the flux of electrons at a variety of energies (effectively the rate at which electrons of different energies were encountered). This showed dramatic step-like changes when Mariner 10 crossed boundaries between

the ambient solar wind environment and the region of space close to Mercury controlled by its magnetic field.

2.3.7 *Charged Particles*

This experiment used two charged particle telescopes to detect high-energy particles (mainly electrons, but also protons and helium nuclei). These were copies of the instruments that had been launched shortly before on Pioneer 10 in March 1972 and Pioneer 11 in April 1973 to fly past Jupiter (Jan 1974 and Jan 1975) and Saturn (Oct 1979). They complemented the Magnetic Field and Plasma Science experiments in revealing phenomena associated with Mercury's magnetic field.

2.4 Mapping a New Planet

2.4.1 *Quadrangles*

Before Mariner 10 arrived, preparations were made for mapping Mercury's surface. Images from the television science experiment were to be used as a basis for both pictorial terrain maps and interpreted geological maps. The prime meridian (0° longitude) of Mercury had already been defined as the longitude where the Sun was overhead when Mercury passed through its first perihelion in the year 1950. A glance back at Fig. 1.7 shows that this must coincide with one of the planet's 'hot poles'.

The surface of a planet or a large moon is conveniently divided into 'quadrangles' for mapping purposes. For Mercury, the Astrogeology Branch of the United States Geological Survey devised a system of five equatorial quadrangles to be mapped on Mercator projections, four northern and four southern quadrangles to be mapped on Lambert projections, and two polar sheets to be mapped on polar stereographic projections (Fig. 2.7). The quadrangles are numbered H-1 to H-15 (where H is a prefix to signify Mercury, from the Greek Hermes). Original IAU-approved names for each of these quadrangles were taken from the albedo features on the Dollfus-Antoniadi map (Fig. 1.6). However, it was found that these albedo features are not apparent in close-up images, so new names were devised for the quadrangles taken from the name of a prominent feature in each quadrangle revealed by Mariner 10, once such features had been named.

2.4.2 *Naming Features*

The naming of specific features on a planet that no one is likely to visit is a far from pointless exercise. It is much more convenient to have names that all concerned

Mercury

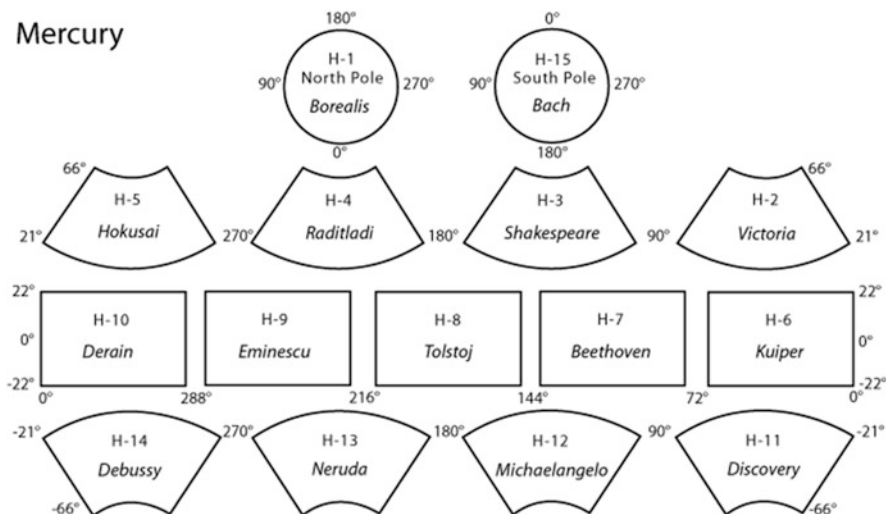


Fig. 2.7 The mapping quadrangles for Mercury, showing the currently-agreed names. Mariner 10 did not image the six westernmost quadrangles, so until MESSENGER images became available these still went by their pre-Mariner 10 names of Apollonia, Liguria, Pieria, Solitudo Criophori, Cyllene, and Solitudo Persephones

recognise than it would be if features could be referred to only by their co-ordinates. A present-day use for names unforeseeable in the Mariner 10 era is that if you want to find out what has been published about a particular feature, then its name is the most useful term to feed into an online search engine.

Surface nomenclature is overseen by the IAU, with two principal aims. First, to allocate non-controversial names that achieve a balance representing all the world's cultures, across the Solar System as a whole and, to the extent possible, also on individual bodies. Second, to indicate what class a feature belongs to, but without implying how it formed. The first is intended to avoid names being contentious, and the second tries to avoid names becoming obsolete or inapplicable as a result of new data or reinterpretation.

Following a convention previously established for the Moon and Mars, craters on Mercury are simply given a one part name according to a theme for crater names agreed for the planet. Other features are given two part name: the name itself (according to the theme for each particular kind of feature) plus a descriptor term. The descriptor term denotes the morphological characteristics of the feature, and is derived from Latin. If this seems complicated, Table 2.2 should help.

Craters are by far the commonest named features, with over 370 names allocated to individual craters by late-2014. The next most common named features are Rupes (scarps), of which 30 had been named by late-2014, when there were seven named Planitiae. The only two named Dorsae were Antoniadi Dorsum and Schiaparelli Dorsum, both named on the basis of Mariner 10 images. The descriptors

Table 2.2 The IAU-approved naming convention for features on Mercury

Type of feature	Theme for name	Descriptor term (plural in brackets)
Crater	Famous deceased artists, musicians, painters, authors	(None used)
Chain of craters	Radio telescope facilities	Catena (Catенаe)
Ridge	Astronomers who made detailed studies of Mercury	Dorsum (Dorsa)
Long, narrow depression	Significant works of architecture ^a	Fossa (Fossae)
Mountain	Words for “hot” in various languages	Mons (Montes)
Low-lying plain	Names for Mercury (the planet or the god) in various languages	Planitia (Planitiae)
Scarp	Ships of discovery or scientific expeditions	Rupes (Rupes)
Valley	Abandoned cities/settlements of antiquity ^a	Vallis (Valles)

^aIndicates themes allocated only after MESSENGER images had been acquired

Montes and Fossae had each been allocated once only, both in the plural form. Caloris Montes denotes the uplifted rim-wall fringing the Caloris basin (which is more properly referred to as Caloris Planitia), and Pantheon Fossae denotes a system of radial fractures in the centre of the Caloris Basin that was not recognised until MESSENGER arrived.

There are only a few exceptions to the naming themes. Borealis Planitia means literally Northern Plain and is inherited from the old Borea albedo province, from which the Borealis quadrangle takes its name. Caloris Planitia was so-named (‘Hot Plain’) because it sits astride one of Mercury’s hot poles. The most prominent young bright (high albedo) crater seen by Mariner 10 was named Kuiper, after Gerard Kuiper (1905–1973), a famous Dutch-American planetary astronomer who had been a member of the Mariner Venus-Mercury imaging team but who died shortly after launch.

Most re-named quadrangles are named after a large or otherwise prominent crater that falls within them. The only exceptions other than Borealis are Victoria and Discovery, which are both named after Rupes.

2.5 What Mariner 10 Found

2.5.1 Surface Characteristics

Fast orbital speeds at Mercury’s close distance from the Sun result in typical impact speeds of nearly 90 km s^{-1} for comets and about 34 km s^{-1} for asteroidal material hitting Mercury, as opposed to 50 and 17 km s^{-1} respectively for comet and

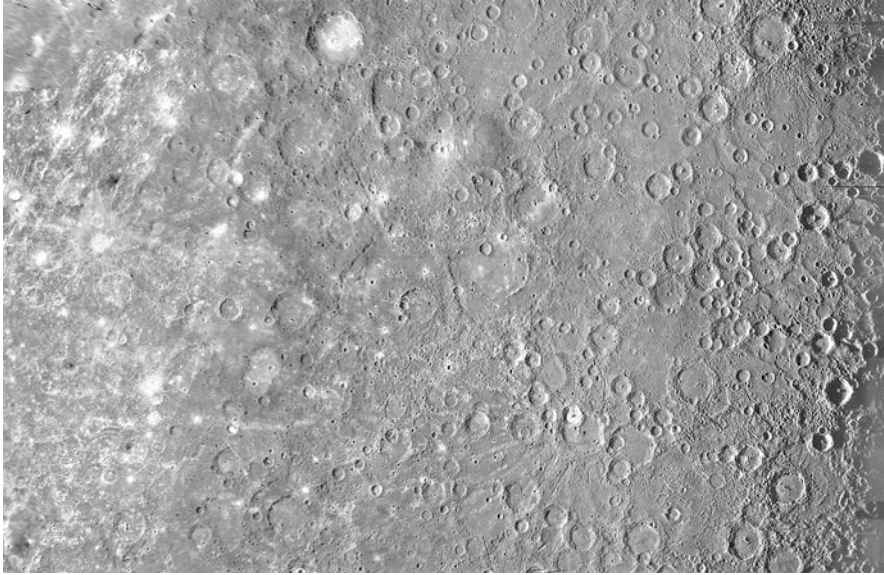


Fig. 2.8 Most of the Kuiper quadrangle, seen in a seamless computer-generated mosaic of Mariner 10 images displayed in a Mercator projection. The area shown is about 2,700 km from east to west. The bright-floored crater in the lower right is Kuiper itself, from which the whole quadrangle takes its name (NASA)

asteroid impacts on the Moon and Earth. It was no surprise that Mariner 10 revealed Mercury as a heavily-cratered planet, given that it was already known to lack sufficient atmosphere to protect its surface. In fact, some larger craters had been seen using Earth-based radar several years before Mariner 10. Figure 2.8 is an overview of the Kuiper quadrangle, where much of the terrain is particularly heavily cratered, though smoother ‘plains’ areas are apparent between craters.

Note how the appearance of craters changes across the wide range of longitudes covered in this view. The eastern edge is on the terminator, experiencing local sunset (very high Sun angle) so craters and various other surface irregularities show up well. The western edge was nearly at local noon (low Sun angle), and there are no shadows. The youngest craters, which are surrounded by high-albedo ejecta, show up as white spots, and they have bright rays radiating from them. Kuiper is probably the youngest crater of its size in this quadrangle and is now known to have rays emanating from it in all directions. However under the Mariner 10 illumination conditions the rays to its west can be discerned only faintly, and those to its east do not show up at all.

Figure 2.9 is a somewhat more detailed view of the northwestern quarter of the Shakespeare quadrangle. This shows wide expanses of plains more clearly than the previous image, and you can also see that the large basins Van Eyck and Shakespeare itself are shallow and have flat floors occupied by smooth, plains-like material (with some smaller, younger craters superimposed).

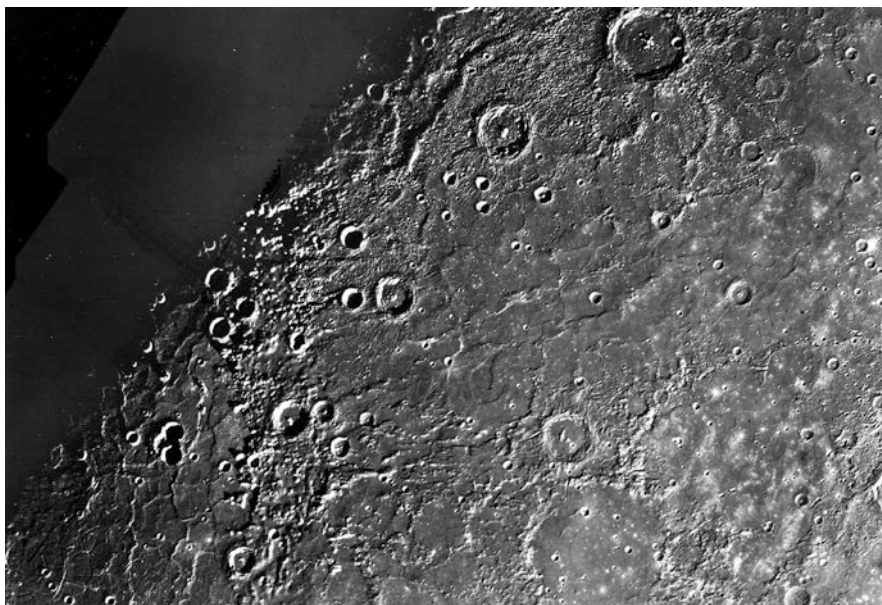


Fig. 2.9 The northwest quarter of the Shakespeare quadrangle, seen in a seamless computer-generated mosaic of Mariner 10 images displayed in a Lambert projection. The area shown is about 1,400 km from east to west. Shakespeare crater, from which the whole quadrangle takes its name, is in the lower right corner, with the more obvious 270 km crater Van Eyck slightly overlapping its southwestern edge. Part of the Caloris basin is seen on the terminator at the lower left (NASA)

Telescopic studies of Mercury's brightness at different phases, and the thermal properties measured by Mariner 10's infrared radiometry experiment, showed that Mercury's surface across virtually the entire globe is powdery, with very little exposed solid bedrock. The surface is thus covered by a metres-thick regolith, consisting of fragments of rock generated and dispersed by impacts on all scales from basin-forming down to micrometeorite impacts. Greater impact speeds on Mercury would tend to result in a smaller average grain size than on the Moon, but essentially Mercury's surface is probably very lunar in appearance (Fig. 2.10). Churning of the regolith by small impacts is one reason why crater rays fade into the background with age.

The single most famous feature on Mercury has to be the Caloris basin (more formally known as Caloris Planitia, though technically this refers only to its interior plains), which is a large impact basin situated at one of Mercury's hot poles, from which it derived its name. It can be seen in the low resolution outbound mosaic in Fig. 2.5, and more clearly in the mosaic of higher resolution frames in Fig. 2.11a. It was estimated on the basis of Mariner 10 images to be about 1,300 km across, but complete imaging by MESSENGER has now shown it to be 1,550 km in diameter. It is both the largest and one of the youngest impact basins on Mercury.

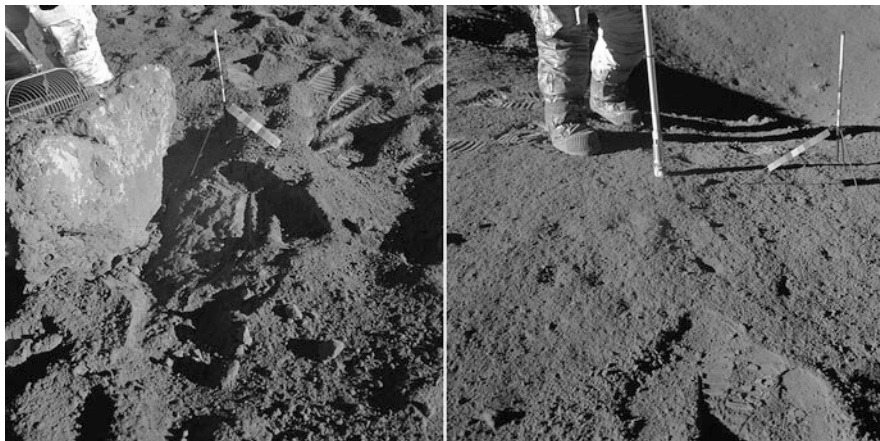


Fig. 2.10 Two Apollo 15 photographs of the lunar regolith. This consists of rock fragments and impact-generated glass on a variety of scales. Particles only tens of micrometres in size make it cohesive enough to retain footprints, but larger fragments are scattered throughout. Mercury's surface would look pretty much the same as this (NASA)

The Caloris basin was clearly formed by a major impact into Mericry, by an impactor that must have been at least 100 km across. It has an uplifted basin rim (Caloris Montes), outside of which much of the terrain has been radially sculpted by what appears to be a mixture of depositional and erosional/abrasional processes during dispersal of ejecta from the impact site. Comparable radial sculpture is associated with some of the impact basins on the Moon, such as Imbrium and Nectaris. The circum-Caloris radial sculpture is overlain by younger plains material, which in places buries it completely. The interior of the basin is completely floored by plains materials, bearing a complex pattern of ridges and troughs, seen clearly in the high-resolution frame in Fig. 2.11b. The fracturing within Caloris is interpretable as a result of uplift of the basement in an isostatic (buoyancy-driven) response to the removal of the excavated material, plus consequences of cooling, contraction and subsidence following emplacement of the basin-filling plains material.

All these features are overprinted by younger impact craters, whose density suggests an age of 3–4 billion years for Caloris itself (during an episode known as the late heavy bombardment, well known from studies of the Moon) to judge from the density of superimposed craters on the Caloris Montes. The Caloris and circum-Caloris plains, which have a lower density of craters, must be younger by up to several 100 million years.

Many scientists working in the Mariner 10 era were happy to accept that the plains associated with Caloris and elsewhere on Mercury (such as Fig. 2.8) are a result of flooding by volcanic lava flows. However, mindful of a recent faux pas when the crew of Apollo 16 visited the supposed volcanic plains of the lunar Cayley Formation in 1972 and found them to be an ejecta sheet, some remained sceptical.

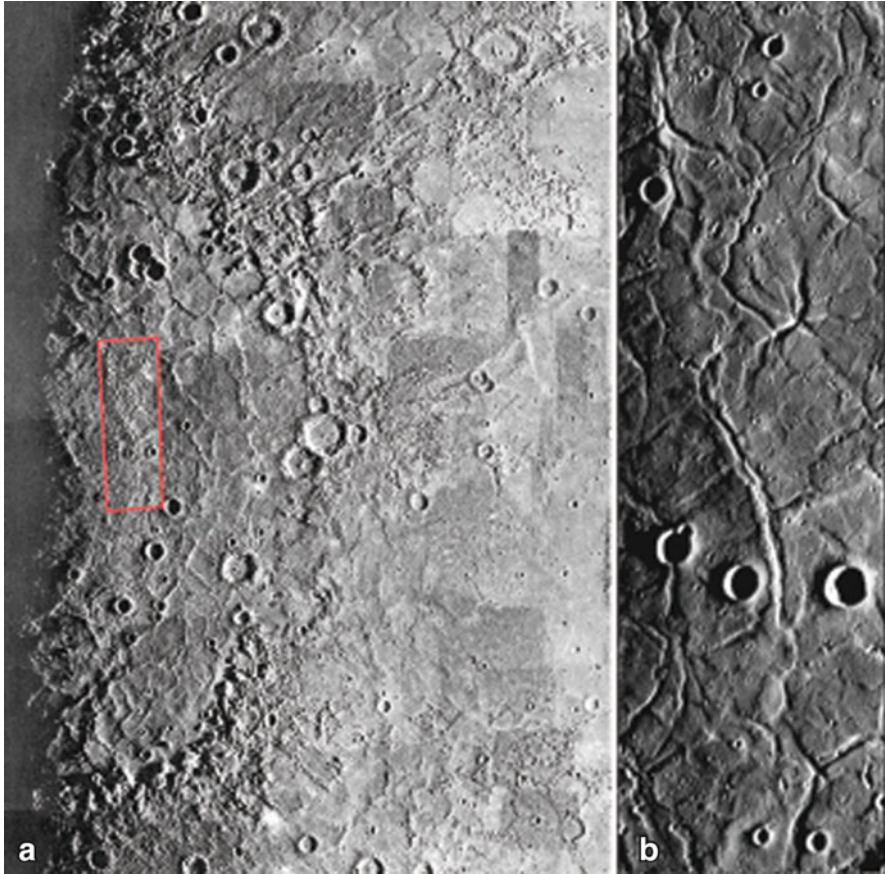


Fig. 2.11 (a) A mosaic of Mariner 10 first flyby outbound images, with most of the individual frames discernible because of incomplete photometric correction between them. The area shown is about 1,100 km across, and the eastern part of the Caloris basin (Caloris Planitia) sits near the terminator at the western edge of the area. The *rectangle* denotes the area shown in (b). (b) High-resolution targeted image strip acquired during Mariner 10's third flyby. The area shown is about 125 km across (NASA)

Smooth plains of impact ejecta remained a defensible interpretation of Mercury's plains until fuller and more detailed imaging by MESSENGER resolved the issue firmly in favour of a volcanic origin.

Like the lunar maria, the plains-forming lavas on Mercury are significantly younger than the basins that they occupy (and beyond which they often extend). The age difference means that eruption cannot be explained simply as a consequence of escape of quantities of pre-existing magma up fractures caused by a large impact. However, unlike the lunar maria, which are significantly darker (lower in albedo) than the lunar highland crust that they overlie (Fig. 2.12), Mercury's lava plains do not contrast strongly with the underlying terrain. This was a (fairly weak)

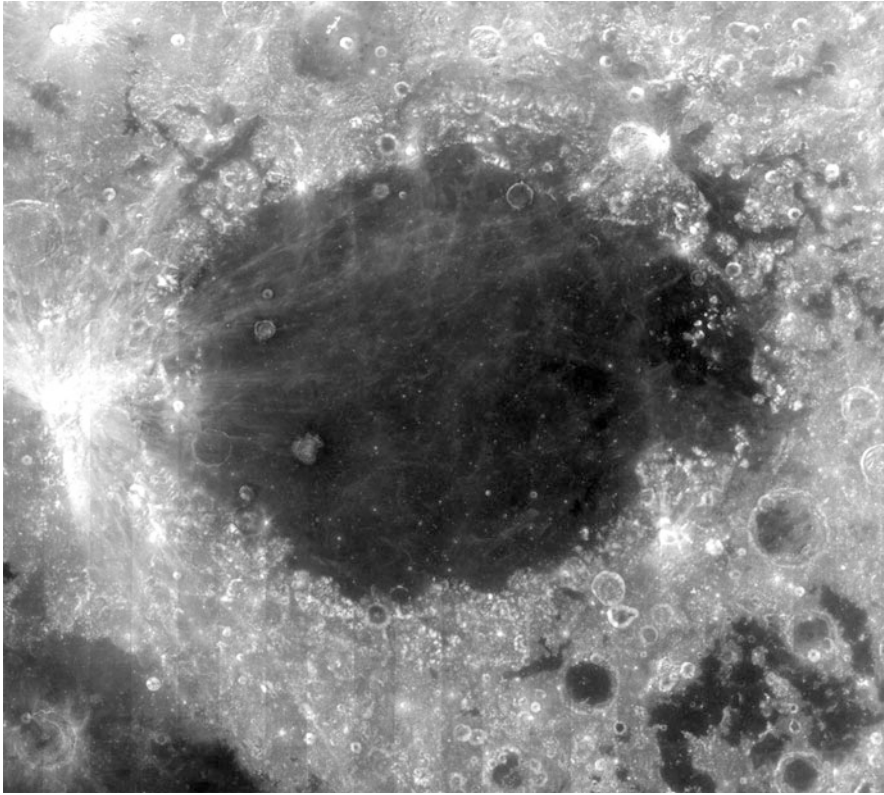


Fig. 2.12 A region on the Moon, about 1,700 km across. This is a mosaic of low Sun angle Clementine images of Mare Crisium and the surrounding region (cylindrical projection). The strong albedo contrast between lunar lava plains (maria) and the older, more heavily-cratered, highland crust is obvious. Such a relationship is absent on Mercury, even at similar low Sun angles (NASA/USGS)

argument in favour of them being composed of the same material, redistributed as ejecta sheets from (unimaged/unidentified) impact sites.

Because the Caloris basin was on the terminator of the Mariner 10 outbound view, the part of the globe exactly opposite, its antipode, was on the opposite terminator, and was seen in Mariner 10's inbound view. The terrain here is unlike anything elsewhere on Mercury, and consists of a jumble of hills up to 1.8 km high (Fig. 2.13). This was dubbed 'hilly and lineated' terrain (though it is more hilly than lineated), and is generally accepted to result from shock waves generated by the basin-forming impact that travelled both through Mercury's interior and round its surface before converging and interfering at the opposite point on the globe. Somewhat similar terrain was recognised about the same time on the Moon, antipodal to the Imbrium and Orientale basins and was explained in the same way.

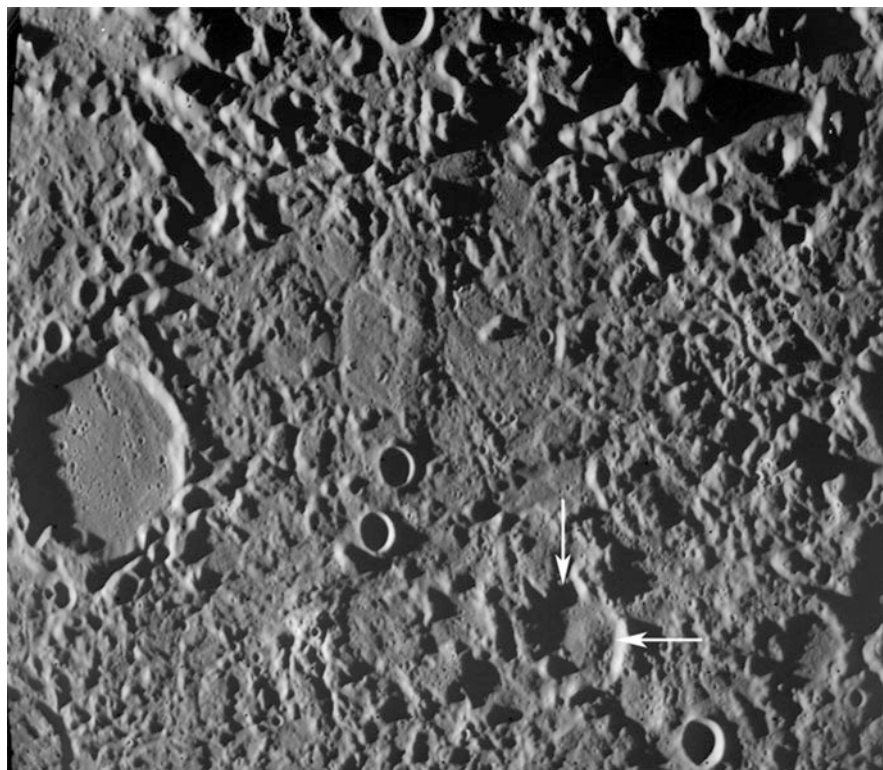


Fig. 2.13 A Mariner 10 first flyby inbound image, 130 km across, which captured ‘hilly and lineated terrain’, antipodal to the Caloris basin. *Arrows* indicate the partially-disrupted rim of a 15 km crater that pre-dates the surface disruption (NASA)

One class of feature revealed on Mariner 10 images that has no analogue (at such a large scale) on the Moon is exemplified by Discovery Rupes in Fig. 2.14, which is named after HMS Discovery – one of the two ships in Captain Cook’s third, and fatal, voyage to the Pacific (1776–1779). The rupes on Mercury are scarps, which is to say steps in the terrain, up to about 2 km high and tens of hundreds of km in length. They are sinuous rather than straight, hence their common description as ‘lobate scarps’.

Lobate scarps cut across all terrain units, and no Mariner 10 image showed plains units embaying any of them. Clearly lobate scarps must be relatively young features, though not so young that they have escaped overprinting by some younger impact craters. Because lobate scarps displace the terrain, they were readily accepted as tectonic features, and specifically as the surface expressions of faults. Moreover, because in plan-view they are lobate rather than straight, it was fairly simple for geologists to recognise them as thrust faults, whose shallow dip intersecting gently rolling topography would naturally result in a wavy line (Fig. 2.15). In some cases there is a measurable shortening of 1–2 km across craters

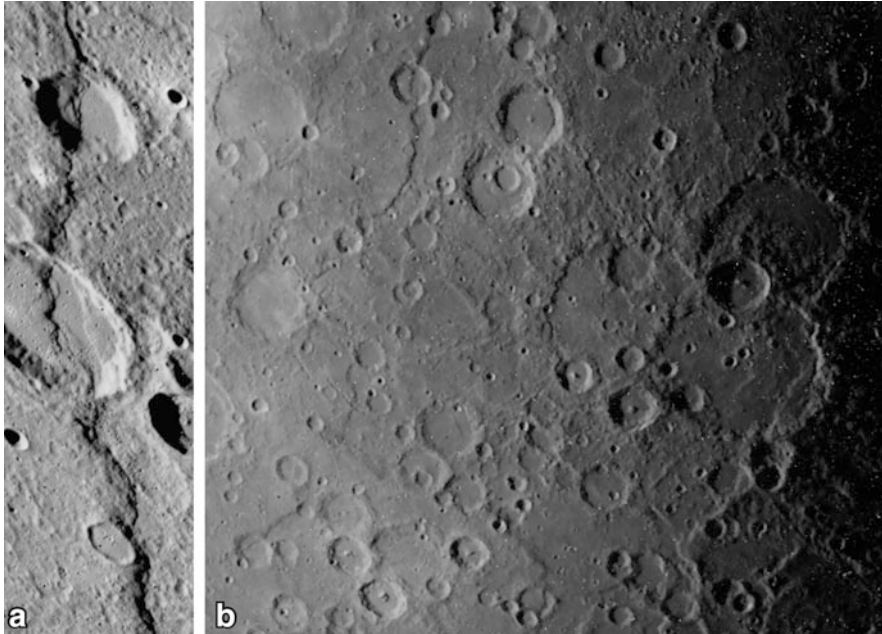


Fig. 2.14 (a) Mariner 10 third flyby high resolution targeted image of Discovery Rupes, which is at about 55° S. The crater Rameau, cut by Discovery Rupes in the centre of the strip, is 31 km across. Note the 8 km crater superimposed on the scarp near the south end of the image strip, whose overprinting relationship shows it to be younger than the scarp. (b) Mariner 10 second flyby inbound image, showing the regional setting of Discovery Rupes. The area covered is about 1,000 km across (NASA)

cut by a lobate scarp, which is consistent with this interpretation. The amount of displacement across a lobate scarp thrust fault is much smaller than for the major thrusts on the Earth associated with continental collision and mountain building, for example in the Alps or the Rockies, where displacement of tens or hundreds of km are known.

In common with faults on the Earth, the displacement across a lobate scarp is presumed to decrease towards the fault-tip at either end of the scarp, and this is consistent with Discovery Rupes becoming less prominent towards its southern tip as is seen in Fig. 2.14b.

Mariner 10 found lobate scarps at a wide range of latitudes, with named Rupes occurring between 49° N and 65° S. There are other tectonic features on Mercury, but I will leave these aside for a fuller discussion in the light of MESSENGER data.

So, what caused Mercury's lobate scarps to form? Before tidal despinning slowed Mercury's probably much faster early rotation to its present 3:2 spin:orbit coupled state, Mercury must have had an equatorial bulge. For example the Earth's equatorial radius is 21 km greater than its polar radius, because of its relatively rapid spin. However, polar and equatorial radii differ by less than 1 km for Mercury today. The collapse of Mercury's former equatorial bulge would have caused a

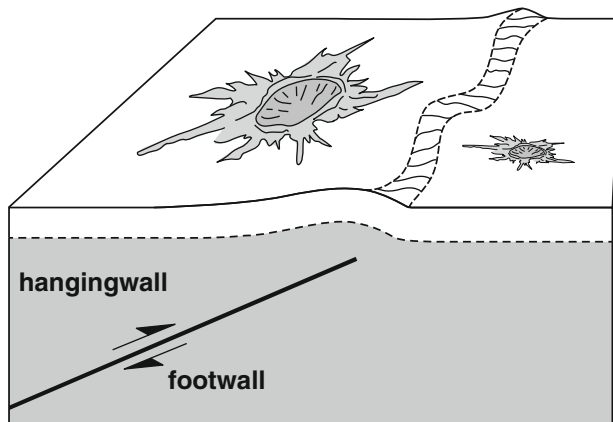


Fig. 2.15 Sketch cross-section to illustrate how a shallow-dipping compressional fault (a thrust fault) can create a lobate scarp at the surface. A steeper fault would result in a more linear topographic feature. The terms ‘footwall’ and ‘hangingwall’ refer respectively to the block of terrain that has been over-ridden by the fault movement and to the over-riding block

reduction in equatorial circumference that would be expected to lead to east–west shortening at low latitudes. However, unless the planet’s total volume decreased, there would have to have been a simultaneous expansion of the polar circumference that should have caused extensional faulting in the polar regions (and strike-slip, sideways, fault movements a little further from the poles). This is inconsistent with the pattern of faulting revealed by Mariner 10, and so it was concluded that tidal despinning must have occurred too early in Mercury’s history to leave such clear traces on its present surface, so another explanation was sought for the lobate scarps.

The overwhelming propensity of tectonic features on Mercury to be compressional in nature led scientists of the Mariner 10 era to conclude that Mercury has been a shrinking planet at all latitudes. Lobate scarps are best seen at high Sun angles, and particularly when the Sun’s direction is such that the downhill side of the scarp casts a shadow. This makes them hard to identify in about half of the region imaged by Mariner 10, and of course none could be seen on the night-side of the globe. However, assuming that the lobate scarps visible on suitable Mariner 10 images are representative of the globe as a whole, they were taken to demonstrate a global contraction in radius of 0.5–1 km.

If a planet is becoming smaller, without losing mass, this requires its density to increase. There are two ways for this to happen, both being consequences of falling internal temperature. One is simple thermal contraction: most solids, including rock, contract as they cool. The other involves internal phase changes, particularly freezing of the core (the solid part of the core growing at the expense of the liquid part of the core), that would cause Mercury’s interior to become denser. In either case,

the rigid rocky outer layer would then be too big to fit over the interior, and it would behave rather like the skin of a desiccating apple, except that it developed mostly asymmetric scarps rather than simple wrinkles.

It is likely that both causes of contraction have operated, and it is possible that late tidal despinning may have had some influence over scarp development too. We will defer further discussion until the MESSENGER data are considered.

2.5.2 Mercury Timescale and Stratigraphy

Those working with Mariner 10 images were quick to follow the recent lead of lunar mappers in looking for evidence to define relative ages of features in Mercury. Relative dating is done using the geologically well-established ‘principle of superposition’, which recognises that overlying or overprinting features are younger than the underlying or overprinted features. The degradation states of the impact craters was also used, on the basis that younger craters would retain their pristine morphology, whereas progressively older craters would lose definition as a result of various processes such as impact gardening (local churning of regolith by small impacts) and partial burial by ejecta from neighbouring younger craters.

Absolute ages of terrains were estimated by counting the density of superimposed craters, and applying the radiometrically-calibrated lunar cratering timescale, after correction for Mercury conditions.

The resulting timescale and stratigraphy, divided by convention into named ‘systems’ (each of which is intended to encompass features and surfaces formed within a specific time bracket) are summarised in Table 2.3. Beware that absolute ages may be significantly in error.

The youngest two systems defined on Mercury were based on isolated craters rather than on extensive surface units. The youngest class of craters in Mercury is typified by the crater Kuiper: morphologically fresh and with associated rays of

Table 2.3 Mercury timescale and stratigraphy, as understood from Mariner 10 data

System	Major units	Age of base/ billions of years
Kuiperian	Fresh craters with rays	1.0
Mansurian	Fresh craters without surviving rays	3.0–3.5
Calorian	Caloris basin and its ejecta	3.8–3.9
	Plains inside and outside Caloris. Partially degraded craters	
Tolstojan	The Tolstoj basin, its ejecta, and associated plains. More heavily degraded craters	4.0
Pre-Tolstojan	Intercrater plains and multiring basins older than Tolstoj. Most heavily degraded craters	>4.0

Tolstoj is named after the Russian author conventionally spelt ‘Tolstoy’, and is usually pronounced that way. Approximate lunar equivalents are (youngest to oldest): Copernican, Eratosthenian, Imbrian, Nectarian, pre-Nectarian

ejecta. Craters like this are probably 1.0 billion years old or younger, and these and any other features of demonstrably similar age are assigned to the Kuiperian system.

The next-oldest system is defined by craters that are still morphologically fresh in respect of the structure of their walls and central peaks. They are surrounded by recognisable ejecta deposits, but lack surviving visible ejecta rays. The crater Mansur is apparently the oldest such example, and the ejecta from Mansur defines the base of the Mansurian system, which began about 3.0–3.5 billion years ago. Mariner 10 showed no surface units of regional extent to which a Mansurian age could be attributed, though the floors of some Mansurian craters have become occupied by smooth material (which must therefore be Mansurian or Kuiperian in age).

Prior to the Mansurian, it is possible to recognise units of regional extent. The youngest of these are assigned to the Calorian system, which begins with the excavation of the Caloris basin (about 3.9 or 3.8 billion years ago) and continues with the smooth plains both inside and outside Caloris that can be shown to post-date the basin. The rims and any internal terraces of impact craters of Calorian age are degraded, and smooth crater-fill is often present. Proximal ejecta deposits can still be seen surrounding Calorian craters. Most of the region covered in Fig. 2.9 is plains of Calorian age.

The next oldest system is the Tolstojan, which begins with the formation of the 510 km diameter Tolstoj basin (Fig. 2.16), about 4.0 billion years ago. This may have been as little as 0.1 billion years before the Caloris basin, so the Tolstojan

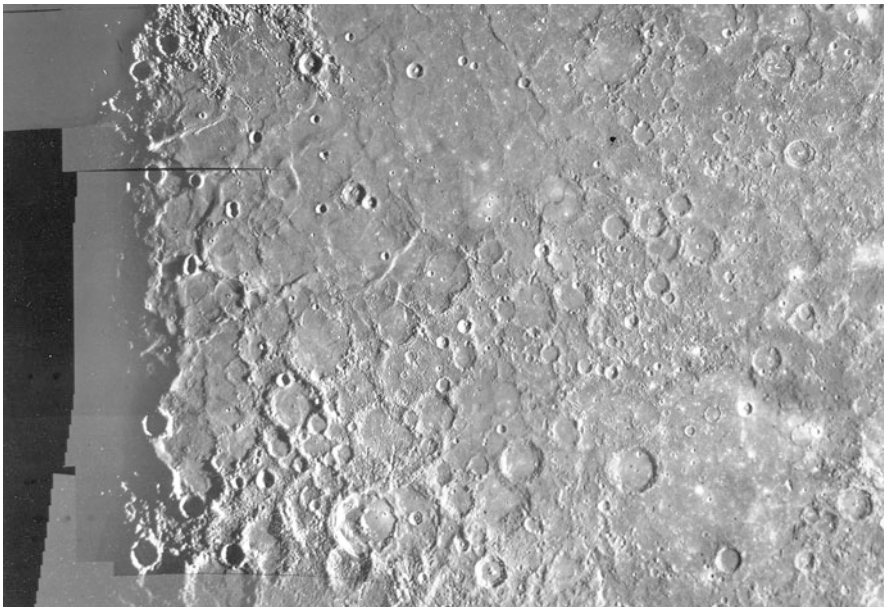


Fig. 2.16 Mariner 10 mosaic covering about 1,200 km east to west, and showing Tolstoj basin in the southeast. The surrounding plains are pre-Tolstojan intercrater plains, except for some Calorian plains in the northwest corner (which lies southeast of the Caloris basin) (NASA)

represents relatively short period of time, but one during which there was a lot of impact cratering (it was during the inner Solar System's late heavy bombardment episode) as well as plains formation. Craters of Tolstojan age have smooth fills, degraded rims, and no surviving proximal ejecta deposits.

Everything older than this is described as pre-Tolstojan. This includes many poorly-preserved impact basins. Whatever early crust these basins were formed in has been largely buried by 'intercrater' plains of pre-Tolstojan age, now generally accepted to be volcanic plains old enough to have been liberally peppered by subsequent impacts. Much of the region shown in Fig. 2.8 is of this type. Nowhere on Mercury is so heavily cratered as the lunar highlands, and the nature of the very oldest crust of Mercury remains a mystery.

2.5.3 The Magnetic Field

Mariner 10 made just two passes through Mercury's magnetosphere (the zone within which the paths of charged particles are controlled by the planet's own magnetic field rather than the Sun's), and both were on the night-side of the planet. Despite the limitations of such restricted coverage, a credible general model for Mercury's magnetic field was developed by combining data from the Magnetic Field, Plasma Science and Charged Particles experiments (Fig. 2.17). The total

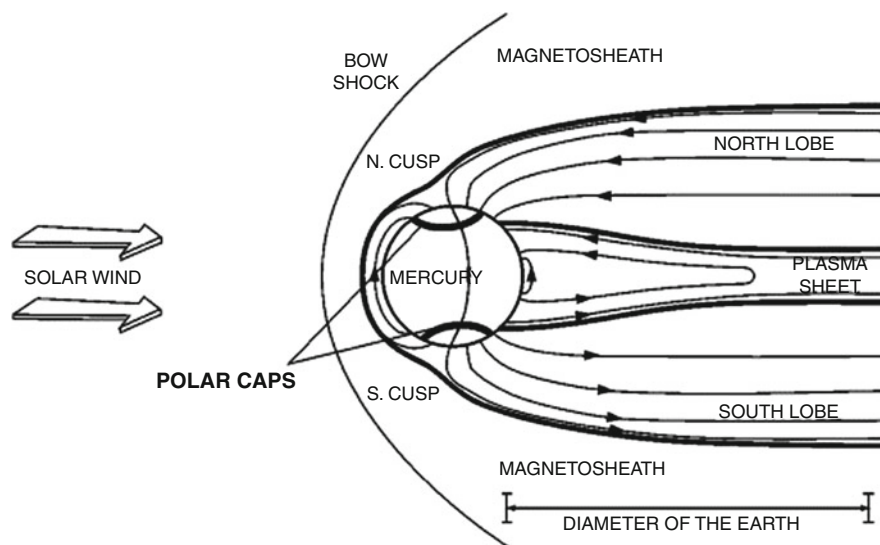


Fig. 2.17 A post-Mariner 10 model of Mercury's magnetosphere, showing magnetic field lines and labeled regions. This model is still reasonably valid, except that MESSENGER revealed a north-south asymmetry, such that the field is displaced northward of Mercury's equator by about one-fifth of the planetary radius (Modified from Grad, E., and Balogh, A., *Planetary & Space Science*, v.49, pp.1395-1407, 2001)

strength of the field is about 1 % of the Earth's, with which it shares many characteristics except that the solid body of Mercury occupies a much greater proportion of its magnetosphere than the Earth does.

Essentially Mercury's magnetic field resembles that of a giant bar magnet, aligned along the planet's spin axis, described as a dipole. It is distorted because of the overpowering influence of the solar wind, which consists of charged particles (mainly electrons and protons) streaming away from the Sun at hundreds of kilometres per second. The magnetopause is the boundary where the pressure from the planetary magnetic field is balanced by the pressure from the solar wind, or, in other words, where the field lines of the Sun's magnetic field are held at bay by the field lines of the planet's own magnetic field. Based on the two Mariner 10 passes through the magnetosphere, the magnetopause was assumed to be only about half a planetary radius above the (unvisited) day-side, but to extend much further on the night-side in a 'magnetotail' where a sparse flow of charged particles is able to be channelled 'upstream' along the magnetic field lines in the opposite direction to the solar wind. Mariner 10 passed through the plasma sheet, in the equatorial part of the magnetotail, where the field is weak but the density of charged particles is much higher. It was speculated that at times of high solar activity, the day-side magnetopause would probably be forced down to the planetary surface.

The outer limit of the magnetosphere is the bow shock, where solar wind particles experience sudden deceleration (from supersonic to subsonic) as they approach the magnetopause. Between bow shock and magnetopause lies the magnetosheath, marked by slow (subsonic) solar wind mixed with some plasma from the magnetosphere.

2.5.4 The Interior

Of course there is not actually a giant bar magnet inside Mercury. Nor is its iron core 'magnetised' in any way – the internal temperature must be far too hot for any kind of 'permanent magnet' (the Curie temperature of iron, above which it cannot retain a magnetic field, is 770 °C). The only known way for a terrestrial planet to generate its own magnetic field is by motion within a liquid, electrically conducting layer, which acts as a self-sustaining dynamo. This is fairly well understood in the case of the Earth, where seismic data clearly show that the outer core is liquid (molten). Mariner 10's discovery of Mercury's intrinsic magnetic field showed that it was likely to have a liquid shell in its core too, although it had been unexpected and there was no other compelling evidence for the size, or the location, of the molten zone in Mercury's core.

Confirmation that Mercury's outer core is indeed liquid came in 2007, with the publication by Jean-Luc Margot and colleagues of their analysis of simultaneous radar observations from California, West Virginia and Puerto Rico during 2002–2006. Matching up the speckled pattern of the radar echo from Mercury's Earth-facing hemisphere at two different receivers enabled tiny variations in Mercury's spin rate to be measured, revealing libration of Mercury's surface amounting to a

few hundred metres of side-to-side wobble during each orbit. This may seem tiny, and it was a remarkable feat to detect it, but it is a much greater libration than could occur if Mercury were solid throughout. However, it is entirely consistent with the solid rocky part of the planet being decoupled from the main body of the core by a liquid shell occupying the outer core. Modelling suggests that such a liquid shell could be prevented from freezing if it contained a few percent of sulfur. Motion in this shell is likely to be maintained not so much by Mercury's rotation but by convection as metal freezes onto the top of the inner core, making the residual outer core progressively richer in sulfur and so more buoyant.

As established in Chap. 1, the rocky part of Mercury surrounding its core is relatively thin – accounting for the outer 25 % of Mercury's radius (so about 600 km thick according to pre-MESSENGER models) and 58 % of its volume. In contrast, Earth's rocky part occupies the outer 44 % of its radius and 84 % of its volume. Mariner 10 provided no data on the structure of the rocky zone, but by analogy with the Earth it was expected that the majority would be classifiable as 'mantle', made of silicate rock of a composition broadly similar to the rock known on Earth as peridotite (with a chemical composition of approximately 45 % SiO_2 , 38 % MgO , and the remainder mostly oxides of iron, calcium and aluminium). Overlying this, in a surface shell a few tens of km deep, would be Mercury's crust, composed of silicate rock poorer in MgO than the mantle, but correspondingly richer in the other common oxides. The crust would be naturally slightly lower in density than the mantle, having been extracted from it by a variety of possible processes soon after the birth of the planet. These processes could include crystallization from a global magma ocean, and volcanic eruption and igneous intrusion after the mantle had solidified. Figure 2.18 illustrates the internal layered structure of Mercury as understood after Mariner 10. Box 2.1 defines terms in general use to denote layers within a planet.

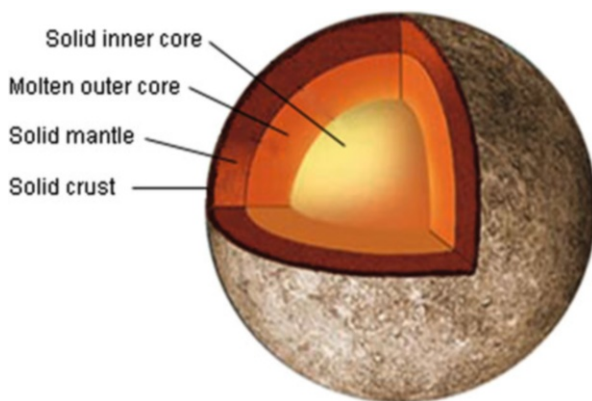


Fig. 2.18 The basic internal structure of Mercury, as understood after Mariner 10. The inner core is probably mostly iron with a few percent nickel, whereas the molten outer core must contain also a lighter element such as sulfur, capable of suppressing the freezing temperature. The mantle and crust are rocky, being composed of silicate minerals

Box 2.1. Terminology for Planetary Interiors

Planetary scientists use a small number of terms to denote layers within a planetary body. These are defined here for the benefit of readers who may be unfamiliar with them.

Core: a compositionally distinct dense inner part. In the case of terrestrial planets the core is thought to be metallic: mostly iron with a few percent nickel. If the outer part of the core is liquid (as in the case of the Earth and Mercury) this is believed to occur because of the presence of a lighter element, such as sulfur, capable of reducing the melting temperature. Earth and Mercury thus have a solid inner core and a liquid outer core.

Mantle: whatever surrounds the core. In the case of a terrestrial planet this is made largely of silicate minerals, based around silicon atoms each bonded to four oxygen atoms, SiO_4^{4-} , with the charge balance maintained by the presence of ions of various metallic elements, chiefly Mg, but also Fe, Ca, Al, Ti, Na, K (magnesium, iron, calcium, aluminium, titanium, sodium, potassium).

Crust: a differentiated, and potentially heterogeneous, layer enclosing the mantle, from which it has been extracted by various processes. In terrestrial planets the crust tends to be richer than the mantle in all the elements listed above except Mg, which is much less abundant in crust than in mantle. Crust can form by flotation of low-density crystals in a magma ocean (primary crust, like the lunar highlands) or be supplied by volcanic eruption and igneous intrusion of magmas extracted from solid mantle by partial melting (secondary crust, like the lunar maria and the Earth's oceanic crust). Partial melting does not fractionate Fe strongly, so secondary crust has only slightly higher Fe content than the mantle from which it was extracted.

Whereas core, mantle and crust are defined on the basis of compositional differences, it is also useful to recognize mechanical layering too. The elastic outer layer of a planetary body is its **lithosphere**. In the case of the Earth this comprises the crust and the uppermost part of the mantle jointly comprising a rigid shell that is 20–50 km thick in the oceans and about 150 km thick in the continents. The lithosphere can be defined by its rigidity in response to stress (it appears thicker for faster stress rates) or as a conductive lid (where heat is transferred purely by conduction) above a more mobile, convecting interior.

Below the lithosphere, the mantle although essentially solid is capable of flow at rates of a few cm per year. In this part of a planetary interior, heat is carried outwards by convection. The convecting part of the Earth's mantle is weakest immediately below the lithosphere and this is described as the **asthenosphere**. Other planets appear to lack an equivalent especially weak zone, but for many purposes the whole of the convecting part of a mantle can be treated as asthenosphere.

2.5.5 *Surface Composition*

None of the instruments in Mariner 10's experiment suite were tailored towards determining the composition of Mercury's surface. Measurements of how the brightness of sunlight reflected by the surface varies at different phase angles (the angle between the Sun, the surface, and the observer) by Mariner 10 and by Earth-based telescope instruments suggested that the topmost millimetre of Mercury's regolith is finer and more translucent than the lunar regolith, and probably contains more agglutinate particles (tiny fractured grains stuck together by impact-glass). The small particle size and the amount of agglutinates are plausible consequences of the higher impact energies at Mercury, whereas the degree of translucency is consistent with the surface paucity in iron that is inferred by other means (as described shortly).

Mariner 10's airglow spectrometer showed that Mercury's albedo (the fraction of incident sunlight reflected) is a few percent lower than the Moon's in the extreme ultraviolet. Mercury's albedo in the visible part of the spectrum is also slightly lower than the average for the lunar near-side. However, Mercury's reflectance rises more steeply with wavelength than the Moon's, so that Mercury is more reflective than the Moon at near-infrared wavelengths. Another way of putting this is to say that Mercury is slightly redder than the Moon, though this is too subtle an effect to be the main reason behind Mercury's 'pale pink dot' visual appearance.

Reflected light spectroscopy and emitted infrared spectroscopy (both of which can be attempted with telescopes) were among the few techniques, prior to MESSENGER, capable of giving information on the mineralogic composition of Mercury's surface. Most notably, iron in silicate minerals will absorb light in the 900–1,100 nm region as the result of electron transitions (between energy states) in iron atoms bonded to oxygen. The wavelength of the deepest part of the absorption depends somewhat on the size and shape of the crystal lattice surrounding the iron atom, and so if the depth and central wavelength of this feature can be identified it places constraints on both the amount of iron in silicates and on the species of minerals in which most of the iron occurs. In the event, this iron feature proved elusive, and the consensus arrived at prior to MESSENGER was that FeO in silicates could not be more than about 3 % by weight (wt%). Hints of an absorption feature near 1,100 nm suggested that such iron as is present occurs mostly within the mineral clinopyroxene. Mid-infrared spectra, obtained from the summit of Mauna Kea in Hawaii to minimise absorption by atmospheric water vapour, showed some regional variations across Mercury's surface and were consistent with 3–5 wt% FeO. Untangling the possible mixtures of minerals that could be responsible for the spectrum was fraught with uncertainties, but feldspars and magnesium-rich, iron-poor pyroxenes of the clino- (Ca-bearing) and ortho- (Ca-poor) varieties seemed likely.

Disc-resolved microwave imaging provided a further insight by measuring Mercury's 'dielectric loss tangent', which constrained the total FeO + TiO₂ content of the surface to be <6 wt%. In the 1990s this was misinterpreted as indicating that

most of Mercury was covered by feldspar-dominated rocks, possibly anorthosite analogous to the lunar highland crust, whereas it became clear thanks to MESSENGER that much of Mercury's surface is Mg-rich (and very Fe-poor) lavas made largely of pyroxenes plus 20–30 % of feldspar.

2.5.6 *Space Weathering*

The very limited colour imaging by Mariner 10 showed some regional variations, but was useful chiefly to demonstrate that the spectral properties of Mercury's surface change over time in a manner similar to that already understood for the Moon, though probably faster because of Mercury's more extreme environment. These changes are a result of 'space weathering', a blanket term encompassing a variety of processes affecting the physical and chemical (and hence the optical) properties of any airless body (Fig. 2.19).

Meteorite and micrometeorite bombardment vaporises some of the target, pulverises more of it, and embeds particles in glass-welded agglutinates, as previously mentioned. High energy cosmic rays and solar ultraviolet light can break vulnerable chemical bonds (a process called 'photon-stimulated desorption'), and release atoms into space, thus changing the surface composition. Solar wind particles (electrons and ions) can also eject atoms (a phenomenon described as sputtering), but they can also become trapped (implanted) into the surface, changing the

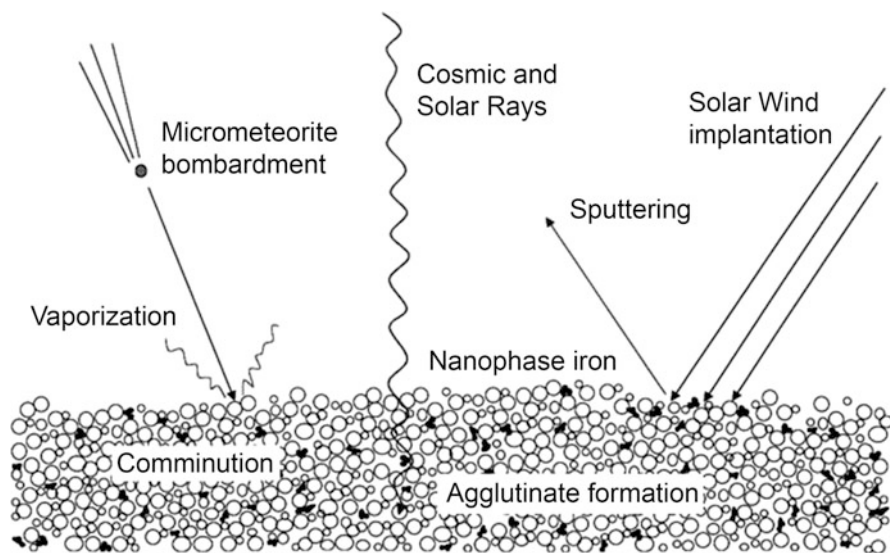


Fig. 2.19 The different components of space weathering (Modified after: Sarah Noble, creative commons)

composition by addition as well as by subtraction. The mixing of meteoritic material into the regolith will also change its composition over time.

A major result of space weathering on the Moon is to break iron-oxygen bonds and embed particles of metallic iron within the agglutinates and on exposed surfaces of minerals. These particles are typically a few nanometres in size, and so they are described as nanophase iron. Nanophase iron has the effect of darkening and reddening the overall spectral response of the regolith. On the other hand, increasing abundance of spectrally neutral opaque minerals, such as ilmenite (FeTiO_3), is found to darken the material but also to make it less red.

A plausible reason why Mercury is darker (has a lower albedo) than the Moon could be that the regolith is rich in ilmenite, which is why the upper limit on the total $\text{FeO} + \text{TiO}_2$ provided by microwave measurements was important, and showed that a different explanation must be sought.

2.5.7 *The Exosphere*

Mercury's gravity is too weak and its day-side temperature too high to enable it to retain a dense atmosphere. Although it does have some atoms gravitationally bound to it, these are too few and far between to collide with each other, so they just bounce around on large, parabolic ballistic trajectories. At their furthest from the planet, they are vulnerable to being swept away by the solar wind or simply by the pressure exerted by solar radiation. The same situation prevails in the outer part of the Earth's atmosphere, in the zone known as the exosphere. However, unlike the Earth, Mercury's exosphere extends right down to the surface, so it is described as a 'surface-bounded exosphere'.

Mariner 10 provided the first data on Mercury's exosphere, when measurements by its UV airglow spectrometer were used to calculate the density of atomic oxygen, helium and hydrogen (O, He and H) to be about 44,000, 6,000 and 230 atoms per cubic cm at the planetary surface, respectively. What was actually measured was the column density of each species (the total number of atoms along a line of sight), which was then modelled down to the surface assuming hydrostatic equilibrium.

Mercury's ground-level density of oxygen atoms at 44,000 per cubic cm might seem like a lot, but the density of molecules at the base of the Earth's atmosphere is more than 10^{18} per cubic cm, or at least 10^{13} times greater than on Mercury. Another useful comparison is given by the atmospheric pressure at the surface. Mercury's surface atmospheric pressure is about only 10^{-15} of the Earth's.

The most straightforward way to account for the exospheric H and He detected by Mariner 10 is capture from the solar wind, though inevitably some He must also leak from the surface as a result of radioactive decay. On the other hand the O seemed likely to have been liberated from silicate minerals at the surface by charged particle sputtering.

Table 2.4 Atoms in Mercury's exosphere as known prior to the MESSENGER mission

Species	Column abundance/atoms per cm ²
H	5×10^{10}
He	2×10^{13}
O	7×10^{12}
Na	2×10^{12}
K	1×10^{10}
Ca	1×10^9

To the three species detected by Mariner 10, ground based spectroscopy added sodium (Na) and potassium (K) in the 1980s and calcium (Ca) in 1998. Na was found to have a surface density almost as great as O, whereas K and Ca seemed to be about a hundred and a thousand times less abundant, respectively. These data also revealed the first asymmetries and temporal variations in Mercury's exosphere, with both Na and K varying by an order of magnitude between different observations of the same region of the planet. A dawn-dusk asymmetry was noted, whereby Ca and K are more abundant near the dawn terminator than near the dusk terminator, and Na is more abundant near the poles than near the equator. Ground based spectroscopy also revealed that Mercury has a sodium tail, consisting of atoms stripped out of the exosphere by the pressure of solar radiation and traceable for 50,000 km down-Sun from the planet.

The inventory of Mercury's exosphere as understood before MESSENGER is summarized in Table 2.4, in the form of column abundance (or column density) of the six known species. This is the total number of atoms in a column all the way down to the surface, and the relative values do not compare directly with surface density because of the different scale heights (the rate at which density falls off with height) for species of different atomic masses.

To maintain the exosphere in an approximately steady-state, species must be being removed at a time-averaged rate equivalent to that at which they are supplied. Maybe churning of the regolith is adequate to refresh the supply of rocky material that has not yet lost a significant proportion of the vulnerable elements. Maybe many of the exospheric atoms get reimplanted back into the surface.

Neither the sources nor the sinks of the non-solar wind species were resolved prior to MESSENGER. Photon stimulated desorption, electron stimulated desorption and ion sputtering (during interludes when the magnetosphere fails to adequately protect the surface), thermal desorption and impact vaporization (mainly from micrometeorite impacts) were all suggested as source mechanisms. At least half the loss can be accounted for by photoionization, whereby solar UV ionizes the neutral atoms, some of which are then swept away in the magnetospheric and solar wind currents, whereas others are recycled to the surface and neutralized.

2.5.8 Polar Ice?

To complete the pre-MESSENGER survey we turn again to ground-based radar. As previously mentioned, radar imaging, chiefly using the Arecibo dish, is able to image some of Mercury's craters, and it became apparent that there is something strange about the craters near both of the planet's poles (Fig. 2.20).

The floors and pole-facing walls of craters near the poles reflect an anomalously strong fraction of the incident radar signal, with polarization properties indicative of 'volume scattering', meaning backscatter within a medium rather than specular reflection from a surface. It was quickly suggested that the most likely cause of this was grains of ice (specifically water-ice) within the local regolith. These 'radar bright' locations coincide with permanently shadowed areas (remember that

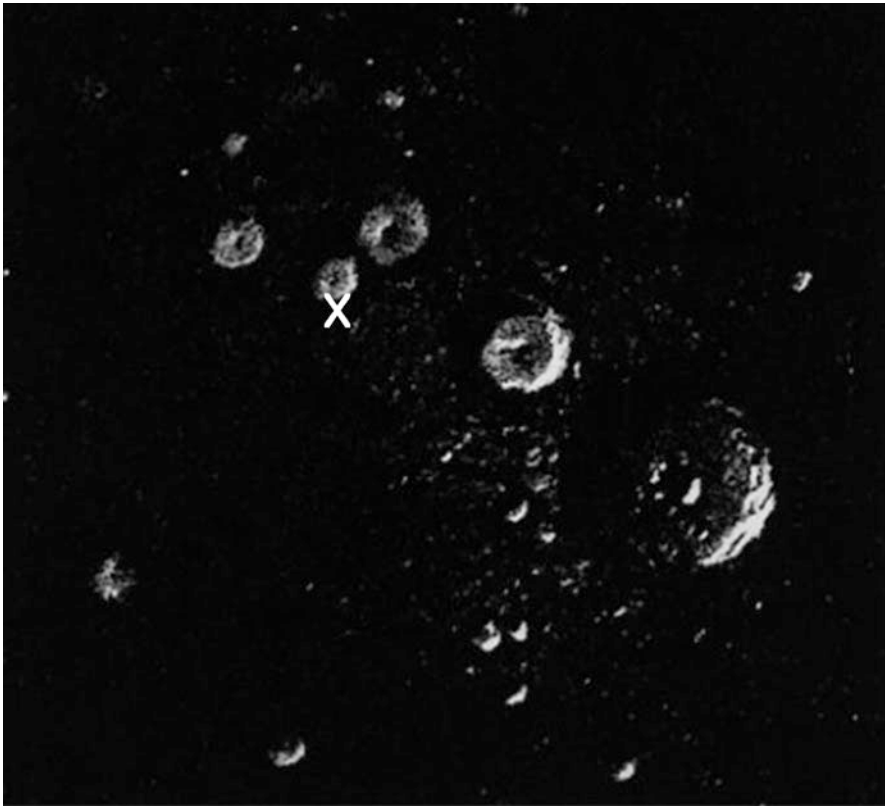


Fig. 2.20 An Arecibo radar image including Mercury's north pole, captured in July 1999. The pole is indicated by the superimposed X. The largest crater in the lower right is 90 km across. Note the bright radar returns on the floors and particularly the pole-facing walls of the craters (From J.K. Harmon et al., *Icarus*, v.149, 1–15, 2001)

Mercury's spin axis has no measurable tilt), so they act as 'cold traps'. When a comet hits Mercury and is vaporised, water molecules will bounce around until dissociated into H and O. However a few molecules will find their way into such a cold trap before they are dissociated, where the very low surface temperature absorbs their kinetic energy upon impact so that they stick rather than bouncing away.

Sulfur has sufficiently similar properties to be indistinguishable from water-ice based on these radar observations alone, and it was not until MESSENGER arrived that the identity of the radar-bright material was confirmed as water-ice.

2.6 The Conundrum of Mercury's Origin

The knowledge gained about Mercury during the Mariner 10 era left us with many conundrums about Mercury's origin. Mercury stood revealed as denser than the other terrestrial planets, with a disproportionally large core relative to its silicate outer layers. How could such a planet form? Was its crust really so deficient in iron as the data seemed to suggest? If so, how could that be reconciled with the enormous amount of iron needed to form its core?

Three kinds of model emerged during the 1970s and 1980s seeking to explain Mercury's high core:silicate ratio. 'Selective accretion' models proposed an oxidation gradient during condensation of the solar nebula that led to more metallic iron and less oxidized iron close to the Sun. This sunward enrichment in metallic iron could have been enhanced by the effectiveness of gravitational and drag forces being different on dust grains of different densities, such that lower-density silicate grains were preferentially removed from the zone where Mercury formed.

Alternatively, 'post-accretion vaporisation' appeals to intense radiation (electromagnetic and solar wind particles) from the young Sun as a cause of vaporisation and loss of silicates from Mercury's exterior after the planet had formed. This process could have worked equally well at an earlier stage, stripping away part of the silicate mantle from differentiated planetary embryos that would later collide and coalesce to form Mercury.

The third kind of model called for the proto-Mercury to have been struck catastrophically by a planetary embryo in a giant impact that stripped away any early crust and part of its mantle (Fig. 2.21). Models of magma ocean crystallization for a planet the size of Mercury suggest that Fe and Ti would be enriched in the upper part of the resulting mantle, and so removal of the uppermost mantle would seem to be consistent with Mercury's crustal deficiency in those two elements, which is probably symptomatic of almost equally low Fe and Ti in the current mantle.

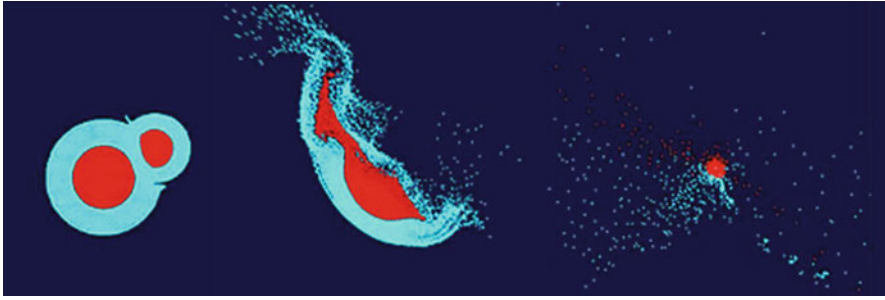


Fig. 2.21 Snapshots of a computer simulation of a Mercury-forming giant impact. *Left*: 2 min after first contact between two colliding planetary embryos, seen in cross-section. Before collision, both were differentiated into iron core (*red*) and silicate mantle (*blue*). *Middle*: the same two bodies 6 min later. *Right*: 2 h later, and shown at half the scale, the core of the target body has been stripped of most of its mantle, only some of which will re-accrete. Most of the dispersed material of dust-size will spiral towards the Sun (From W. Benz et al., *Space Sci Rev*, v.132, 189–202, 2007)

Deciding between these competing models required more data than was available in the pre-MESSENGER era. Indeed, in revealing Mercury's surface to be rich in volatiles, MESSENGER has blown holes in all three models. We will return to this later, but first the next chapter looks at how a new generation of missions to Mercury came about.

Planet Mercury

From Pale Pink Dot to Dynamic World

Rothery, D.A.

2015, XIII, 180 p. 103 illus., 57 illus. in color., Hardcover

ISBN: 978-3-319-12116-1